# Robust design of piezoelectric energy harvesters using polynomial chaos expansions and multi-objective optimization

Paulo H. Martins[1], Marcelo A. Trindade[1], Paulo S. Varoto[1]

[1]*Department of Mechanical Engineering, University of São Paulo*
*Av. Trabalhador São-carlense, 400, 13566-590, São Carlos, SP, Brazil*
*paulo.martins@usp.br, trindade@sc.usp.br, varoto@sc.usp.br*

**Abstract.** The generation of electrical energy from mechanical vibrations and using piezoelectric materials is an attractive alternative due to the high density of electrical charge present in these materials. Although energy can be harvested, the design of devices for this purpose must satisfy specific criteria, because the energy available for conversion into electricity is low. This work suggests the robust design of beam type piezoelectric energy harvesters, considering the presence of uncertainties in certain parameters. Thus, the study presents a finite element cantilever beam model and, through multiobjective optimization, designs the energy harvesting devices to maximize the mean power and minimize the relative dispersion simultaneously. The mean and variance for the frequency response function of the power output are estimated using polynomial chaos expansion. Results show that harvesting devices with smaller length and larger masses generally lead to best nominal performance but also to higher dispersions. Also, the dispersions can be reduced by using effective circuit resistances smaller than the nominal values. With the increase of uncertainties in the parameters of the devices, better performances and decrease in the response variability are achieved by using other design variables in the optimization.

**Keywords:** energy harvesting, multiobjective optimization, uncertainties, robustness

## 1 Introduction

As energy consumption has increased in the last few years, alternative solutions to this problem have emerged. From this perspective, energy can be extracted from wind, thermal, chemical and mechanical sources, for example [1]. Thus, the energy harvested from the vibration in dynamic systems is a motivating alternative. With the use of piezoelectric sensors, the mechanical energy caused by vibrations is converted into electricity. To maximize the energy harvested, it is important that the devices to be properly designed. Figure 1 shows a device with a seismic mass $m_b$, which length is $l_b$, electric resistance $R_c$ and beam lengths $l_v$ and $l_b$. By applying a harmonic input $w_0(t)$ to the base of the device, vibrations will occur, allowing the calculation of power through $R_c$. This value will be maximized when the input and device frequencies are tuned, which is achieved by modifying $m_b$.

Since the amount of energy harvested is generally small, it is important to use optimization methods to design the devices. However, parameters or some design conditions of the devices may present measurement uncertainties or variability [2, 3]. In this case, it is essential to consider the occurrence of uncertainties in the optimization. Optimizations performed in these conditions can be categorized as reliability-based optimizations or robust design optimizations [4]. Concerning the probability of failure and the expected values in the design solutions, we have the first case, while projects that are less sensitive to changes in parameters, loads or some cause are related to the second case.

For robust designs, one way to measure sensitivity is to estimate the mean and variance of the response, allowing the computation of relative dispersion. The response in the case of energy harvesting devices can be the Frequency Response Function (FRF) of output power. However, estimating the mean and variance or statistical moments of a function becomes a challenge when computational cost is a requirement. Monte Carlo Simulations (MCS) are often used for this purpose, but the computational effort is usually high. Consequently, other methods, such as Taylor's first-order series approximations, polynomial chaos and Karhunen–Loève expansions, as well as metamodels, are reasons to study in some works [4, 5].

Multiobjective optimization algorithms are important tools in robust designs because they can simultaneously optimize mean and variance or relative dispersion. For energy harvesting devices, an attractive strategy is to maximize the mean and minimize the relative dispersion of the response. Heuristic algorithms such as the Non-

dominated Sorting Genetic Algorithm (NSGA-II) can be used for this[6]. In multiobjective optimization, multiple solutions are found and the values of their functions are disposed in a curve known as the Pareto front[7]. A particular goal cannot be improved without prejudicing another goal on the Pareto front. The analyst must use certain pre-established criteria to determine the best solution.

In this work, energy harvesting devices will be designed to extract the maximum amount of energy while simultaneously minimizing relative dispersion. The model used is based on finite elements with seismic mass at the end. By applying the NSGA-II method, the multiobjective optimization will be executed, with evaluation of the statistical moments using the polynomial chaos expansion. It is intended to compare three different scenarios for a set of designed devices. In the initial phase, devices with more design variables are designed. Subsequently, the number of design variables decreases, while the uncertain parameters for the new scenario increase. Finally, the most relevant variables and parameters are used in the design of new devices to conclude the last scenario. Through analysis using error bar and Pareto front, conclusions can be reported on the impact of considering more or less design variables or uncertain parameters on the results.
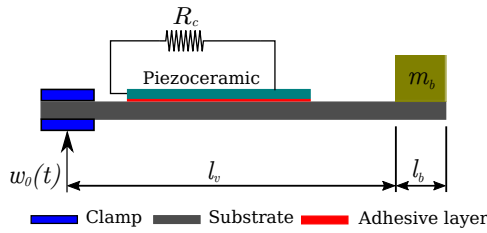


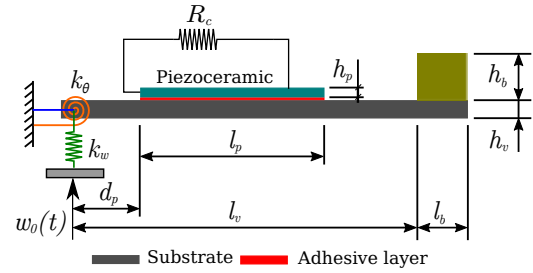Figure 1. Typical model of energy harvesting devices based on resonating cantilever beams.



Figure 2. Schematic representation of the energy harvesting resonant device with imperfect clamp.

## 2 Finite element model for energy harvesting

The finite element model proposed here is based on the work of [8]. With this, a sandwich model was considered for the beam, with two external layers modeled according to the Euler-Bernoulli theory and an internal layer based on Timoshenko's criterion. The piezoelectric material is considered to be perfectly covered with electrodes and composed of orthotropic materials. Figure 2 shows the model to be studied, with an imperfect clamp, simulated by linear springs $k_w$ and torsion springs $k_\theta$. The piezoelectric sensor that is $d_p$ from the clamp is coupled to the beam through an adhesive layer of height $h_c$ and also connected to an electrical resistance $R_c$. The following geometric parameters are considered: length of beam $l_v$ and sensor $l_p$, height of beam $h_v$ and sensor $h_p$, length and height of seismic mass $l_b$ and $h_b$, respectively. Through a harmonic input $w_0(t) = \tilde{w}_0 e^{i\omega t}$, the device will vibrate, allowing to calculate the power generated through the electrical resistance $R_c$. The equations of motion are described as:

$$\mathbf{M}_{rr}\ddot{\mathbf{u}}_r + \mathbf{K}_{rr}\mathbf{u}_r - \bar{\mathbf{K}}_{me}q_c = -\mathbf{M}_{rw}\ddot{w}_0(t), \tag{1}$$

$$R_c\dot{q}_c - \bar{\mathbf{K}}_{me}^t\mathbf{u}_r + \bar{K}_e q_c = 0, \tag{2}$$

where $\mathbf{M}_{rr}$, $\mathbf{K}_{rr}$, $\bar{\mathbf{K}}_{me}$ e $\bar{\mathbf{K}}_e$ are matrices of mass and mechanical, piezoelectric and dielectric stiffnesses. The vectors of relative mechanical displacement and induced electrical charge on the piezoelectric sensor are represented by $\mathbf{u}_r$ and $q_c$, respectively, while $\mathbf{M}_{rw}$ is a column vector with elements of mass. The preceding equations will be modified for modal form by considering $\mathbf{u}_r \approx \phi\alpha_r$, where $\phi$ is obtained through the resolution of the eigenvalue problem $[-\omega^2\mathbf{M}_{rr} + \mathbf{K}_{rr}]\phi = 0$. By incrementing the modal damping matrix $\mathbf{\Lambda}$, we have (1) and (2) written as:

$$(-\mathbf{I}\omega^2 + j2\omega\mathbf{\Lambda}\mathbf{\Omega} + \mathbf{\Omega}^2)\tilde{\alpha}_r - \mathbf{K}_p\tilde{q}_c = \phi^t\mathbf{M}_{rw}(-\omega^2\tilde{w}_0), \tag{3}$$

$$(j\omega R_c + \bar{K}_e)\tilde{q}_c - \mathbf{K}_p^t\tilde{\alpha}_r = 0, \tag{4}$$

where $\mathbf{I} = \phi^t\mathbf{M}_{rr}\phi$, $\mathbf{\Omega}^2 = \phi^t\mathbf{K}_{rr}\phi$ e $\mathbf{K}_p = \phi^t\mathbf{K}_{me}$. $\tilde{\alpha}_r$ and $\tilde{q}_c$ are the modal displacements and circuit electric charges, respectively. The FRF of voltage output will be found by establishing the relationship between resistance and electric current, by $V_c = R_c i_c$, where $i_c = \dot{q}_c$. Therefore, the FRF of output voltage per base acceleration unit will be:

$$G_{Va_0}(\omega) = j\omega R_c\mathbf{K}_p^t\mathbf{D}^{-1}\phi^t\mathbf{M}_{rw}, \tag{5}$$

where $\mathbf{D} = (j\omega R_c + \bar{K}_e)(-\mathbf{I}\omega^2 + j2\omega\mathbf{\Lambda\Omega} + \mathbf{\Omega}^2) - \mathbf{K}_p\mathbf{K}_p^t$.

Similarly, one can find the power dissipated in the electrical resistance by setting $P = V_c^2/R_c$. As a consequence, the FRF of power output per square acceleration input $G_{P\ddot{w}_0}(\omega)$ is written as follows:

$$G_{Pa_0}(\omega) = (G_{Va_0}(\omega))^2/R_c. \tag{6}$$

The equation (6) will be used for the study of energy harvesting, aiming to optimize the devices. Thus, the strategy will be to maximize its mean value and minimize its dispersion simultaneously. Thus, it will be possible to perform all uncertainty analyses and check the performance of the devices.

## 3 Estimation of mean and variance

Given a computational model $\mathcal{M}(\boldsymbol{X})$, depending on a random vector $\boldsymbol{X}$, the response can be expressed using the polynomial chaos, as follows:

$$Y \equiv \mathcal{M}(\boldsymbol{X}) \approx \sum_{\boldsymbol{\varrho} \in A} c_{\boldsymbol{\varrho}}\Psi_{\boldsymbol{\varrho}}(\boldsymbol{X}). \tag{7}$$

In this case, the response was approximated by a sum of terms consisting of deterministic coefficients $c_{\boldsymbol{\varrho}}$ and bases $\Psi_{\boldsymbol{\varrho}}(\boldsymbol{X})$ or multivariate orthonormal polynomials, which are associated with multi-indices $\boldsymbol{\varrho}$. Details on how to find the multi-indices defined as $\boldsymbol{\varrho} = (\varrho_1, \varrho_2, \cdots, \varrho_M), \varrho_i \in \mathbb{N}$, with $M$ random variables, can be found in [9]. The bases $\Psi_{\boldsymbol{\varrho}}(\boldsymbol{X})$ are formed by the multiplication of univariate polynomials dependent on the category of the probability distribution of the random vector $\boldsymbol{X}$. For example, these polynomials are from Hermite, Legendre, and Laguerre for the corresponding random variables with Gaussian, Uniform, and Gamma probability distributions. In addition, random variables have to be standardized for the calculation of polynomial bases.

The set $\mathcal{A} = \mathcal{A}^{M,p}$ is established as $\mathcal{A}^{M,p} = \{\boldsymbol{\varrho} \in \mathbb{N}^M : \|\boldsymbol{\varrho}\|_1 \leq p\}$, where $p$ is the degree of the chosen polynomial, and $\|\boldsymbol{\varrho}\|_1$ is the sum of the terms in the list $\boldsymbol{\varrho} = (\varrho_1, \varrho_2, \cdots, \varrho_M)$. The cardinality of this set will allow to define the number and the bases of the polynomial, and details of how to calculate it can be found [9]. The coefficients can be determined by performing the least squares minimization by finding the argument that minimizes the mean squared error between the difference of the computational model and the one estimated with the truncated polynomial. In this case, a sample set of points $\mathcal{X} = \{\boldsymbol{x}^{(i)}, i = 1, \cdots, n\}$ can be obtained using Monte Carlo method, Latin Hypercube Sampling, Sobol or Halton sequence, for example. The model response will be computed as follows:

$$\mathcal{Y} = \{y^{(1)} = \mathcal{M}(\boldsymbol{x}^{(1)}), \cdots, \boldsymbol{y}^{(n)} = \mathcal{M}(\boldsymbol{x}^{(n)})\}^T. \tag{8}$$

The base of polynomials is used to assemble the following set:

$$\mathbf{A} = \{\mathbf{A}_{ij} \stackrel{\text{def}}{=} \Psi_j(\boldsymbol{x}^{(i)}), i = 1, 2, \cdots, n, j = 1, 2, \cdots, \text{card}(\mathcal{A})\}. \tag{9}$$

where $\text{card}(\mathcal{A})$ is the cardinality of set $\mathcal{A}$. Based on this description, the coefficients will be calculated in the following manner:

$$\hat{\boldsymbol{c}} = (\mathbf{A}^T\mathbf{A})^{-1}\mathbf{A}^T\mathcal{Y}. \tag{10}$$

The mean and variance is easily found after determining the coefficients as follows:

$$\mu_{\hat{Y}} = \mathbb{E}[\hat{Y}] = \mathbb{E}[\sum_{\boldsymbol{\varrho} \in A} \hat{c}_{\boldsymbol{\varrho}}\Psi_{\boldsymbol{\varrho}}(\boldsymbol{X})] = \hat{c}_0, \tag{11}$$

$$\sigma_{\hat{Y}}^2 \stackrel{\text{def}}{=} \text{Var}[\hat{Y}] = \mathbb{E}\left[(\hat{Y} - \hat{c}_0)^2\right] = \sum_{\substack{\boldsymbol{\varrho} \in A \\ \boldsymbol{\varrho} \neq 0}} \hat{c}_{\boldsymbol{\varrho}}^2. \tag{12}$$

By means of (11) and (12), the mean and relative dispersion of the FRF of power output given by (6) are estimated for subsequent optimization with the NSGA-II method.

## 4 Mutiobjective optimization with NSGA-II

The Non-dominated Sorting Genetic Algorithm (NSGA-II) is a method based on the classical genetic algorithm to solve problems with different objective functions simultaneously. For this reason, a population of points in each run of the algorithm is chosen in order to converge towards the Pareto front. In the convergence procedure, the

method seeks multiple non-dominated solutions assigning fitness to the population members and trying to ensure the diversity of points in the final solutions [6].

In the genetic algorithm (GA), the convergence process is divided into stages of reproduction, crossover and mutation based on biological evolution concepts [10]. The variables are manipulated using individuals and a fitness function is evaluated to select the best individuals. By means of probabilistic concepts, the best individuals are selected at the reproduction stage and copies are created to form the mating pool. After this stage, part of the population from the mating pool is chosen and the crossover operator is applied by combining portions of the individuals aiming at producing offspring individuals with better fitness (objective function) values. Finally, the mutation operator is implemented by modifying certain characteristics (properties) of the individuals according to a specified probability. These steps are repeated for a number of generations (iterations) to find the optimal characteristics (design variables) that minimize or maximize a specific objective function.

The stages presented in the genetic algorithm are used in the NSGA-II to find non-dominated solutions and to ensure the diversity in the population. Thus, the first procedure is to rank the individuals by dividing the solutions in fronts or ranks, which are chosen according to the dominance concept. For instance, a hypothetical population can divided in rank 1, rank 2 and rank 3 so that the individuals of rank1 are closer to the optimum Pareto front and should be preferred in the non-dominance procedure. Then, for individuals in the same rank, the diversity of the population is preserved by considering solutions in a less crowded area with the help of an operator that measures the crowding distance.

The initial population with $N$ individuals in NSGA-II is ranked and the operators of reproduction, crossover and mutation are applied to create an offspring population. The new population, which consists of $2N$ individuals, are sorted according to the dominance concept in the best ranks. Also, the crowding distance operator is applied to the individuals in the same rank. Hence, the population is truncated and the best solutions of $N$ individuals are separated, ending the iteration. This process is repeated in order to find the Pareto-optimal solutions based on the number of iterations determined by the end-user.

# 5 Design of robust energy harvesting devices

The design of energy harvesting devices was executed for three different scenarios. The first scenario consisted in the use of a higher number of design variables, the second in more uncertain parameters and the third was composed of the most important variables and parameters in the previous cases. To perform the optimization, some data and parameter values of the devices were defined based on Fig. 2 and in an experimental setup validated in the work of [11]. Some geometric parameters of the validated prototype are: distance between piezoelectric patch and clamp $d_p = 1.1$ mm, piezoelectric patch thickness $h_p = 0.13$ mm, substrate thickness $h_v = 1$ mm, adhesive layer thickness $h_a = 0.08$ mm, substrate length $l_v = 74.7$ mm, piezoelectric patch length $l_p = 73.6$ mm and considering also all parts with 12.8 mm of width. The total effective translation and rotation inertias are estimated as 9.2 g and 0.8 kg mm$^2$, respectively, with length and height of $l_b = h_b = 12.8$ mm. The following piezoelectric coefficients for a sensor PZT-5A of density 7850 kg m$^{-3}$ are: elastic stiffness constant $\bar{c}_{11}^E = 66.3$ GPa, piezoelectric constant $\bar{e}_{31} = 13.3$ C/m$^2$ and dielectric constant $\bar{\epsilon}_{33}^\varepsilon = 12.3$ nF/m. The Epoxy-based adhesive layer has Young's modulus 2 GPa and density 1126 kg m$^{-3}$.

In the first scenario, the corresponding vectors of design variables and uncertain parameters were defined as $\boldsymbol{x}_d = \{l_v, R_c, h_p, l_p/l_v, d_p/(l_v - l_p)\}$ and $\boldsymbol{x} = \{k_w, k_\theta, \zeta, R_c\}$ according to the Fig. 2. For the design variables, if the values of $l_v$, $l_p/l_v$ and $d_p/(l_v - l_p)$ are given, $l_p$ and $d_p$ are determined. Besides the stiffness of the clamp, $k_w$ and $k_\theta$, and electrical resistance $R_c$, the effective damping of the device $\zeta$ is also an uncertain parameter. For all these parameters, the Gamma probability distribution is chosen. Given the above, the FRF presented by (6) is written in terms of $\boldsymbol{x}_d$, $\boldsymbol{x}$ and frequency $\omega$, as follows:

$$Y(\boldsymbol{x}_d, \boldsymbol{x}, \omega) = G_{Pa_0}(\boldsymbol{x}_d, \boldsymbol{x}, \omega). \tag{13}$$

The mean value and variance of (13) are calculated based on (11) and (12). Thus, optimization via NSGA-II is applied to find $\boldsymbol{x}_d$, maximizing the mean and minimizing the relative dispersion of (13). The height of the seismic mass $h_b$ is found by internal optimization, tuning the input and peak vibration frequencies. For all optimizations, a polynomial chaos expansion of degree 3 (PCE-3) was chosen with estimation of the coefficients via Monte Carlo with Latin Hypercube Sampling (MCLHS).

The mean values considered for the uncertain parameters are $k_w = 50$ kN/m, $k_\theta = 0.3$ kNm/rad and $\zeta = 1.1\%$, which are also determined in [11]. The relative tolerance for each variable $k_w$, $k_\theta$, $\zeta$ and $R_c$ was assumed to be 90%, 90%, 10% and 30%, respectively, and equal to three times the relative dispersion. The upper and lower bounds for design variables are equal to $\mathbf{x}_p^L = \{65$ mm, 20 k$\Omega$, 0.13 mm, 0.8, 0$\}$ and $\mathbf{x}_p^U = \{85$ mm, 400 k$\Omega$, 0.25 mm, 0.97, 0$\}$. The input frequency was chosen at 40 Hz, which is very close

to the vibration frequency of the device validated in the cited work. Subsequently, the NSGA-II method was performed with 30 individuals, 150 generations with 70% and 30% of crossover and mutation rates, respectively, to maximize the mean and minimize the dispersion of (13). For this purpose, PCE-3 with 150 samples via MCLHS was used to determine the coefficients in this scenario.

In the second scenario, the vector of uncertain parameters was increased to $\boldsymbol{x} = \{k_w, k_\theta, \zeta, R_c, h_c, E_c\}$, while the vector of design variables $\boldsymbol{x}_d$ was composed only of $l_v$ and $R_c$. The addition was the height of the adhesive layer $h_c$ and the corresponding modulus of elasticity $E_c$ in the vector of uncertain parameters. For defining which of these uncertain parameters most influence the response $h_c = 0.08$ mm ($\delta_{h_c} = 10\%$) and $E_c = 2.0$ GPa ($\delta_{E_c} = 50/3\%$) were defined. Based on the aforementioned experimental design, estimates of mean and relative dispersion with a large number of samples were found using the Monte Carlo method. This allowed to set reference values for the mean and dispersion of the model response equal to $\mu_{\text{ref}} = 41,964$ mW/g$^2$ and $\delta_{\text{ref}} = \sigma_{\text{ref}}/\mu_{\text{ref}} = 10,155\%$. From this, one uncertain parameter was excluded at a time and the mean and dispersion values of the response were verified, being able to compare with the references. For example, $\mu_{k_w^-}$ and $\delta_{k_w^-}$ are the mean and dispersion of response by removing $k_w$, while $\mu_{k_\theta^-}$ and $\delta_{k_\theta^-}$ is the same case by removing $k_\theta$. The results, shown in Tab. 1, indicate that the electrical resistance $R_c$ and the elastic modulus of the adhesive layer $E_c$ are the less influential, according to their corresponding relative dispersion errors $e_r$. Thus, these parameters uncertainties were removed from the subsequent analyses by setting their values to the corresponding nominal values.

Table 1. Output power mean $\mu$ and relative dispersion $\delta$ estimation removing one uncertain variable at a time.

|  | [mW/g$^2$] | $e_r(\%)$ |  | [%] | $e_r(\%)$ |
|---|---|---|---|---|---|
| $\mu_{k_w^-}$ | 42.52 | 1.3 | $\delta_{k_w^-}$ | 8.66 | 14.7 |
| $\mu_{k_\theta^-}$ | 42.63 | 1.6 | $\delta_{k_\theta^-}$ | 8.23 | 18.9 |
| $\mu_{\zeta^-}$ | 41.88 | 0.2 | $\delta_{\zeta^-}$ | 9.48 | 6.6 |
| $\mu_{R_c^-}$ | 42.03 | 0.1 | $\delta_{R_c^-}$ | 10.04 | 1.0 |
| $\mu_{E_c^-}$ | 43.38 | 0.3 | $\delta_{E_c^-}$ | 9.76 | 3.8 |
| $\mu_{h_c^-}$ | 42.09 | 3.3 | $\delta_{h_c^-}$ | 7.50 | 26.1 |

The limits 65 mm $\le l_v \le$ 85 mm and 20 k$\Omega \le R_c \le$ 400 k$\Omega$ were defined and the NSGA-II method applied 30 individuals and 150 generations, maximizing the mean and minimizing the dispersion of (13) in 2nd scenario. In this case, the PCE-3 with 300 samples was used to estimate the coefficients with MCLHS.

Hence, based on the two previous scenarios, the most important design variables were chosen to obtain other devices that could potentially lead to better results despite the increased uncertainties. In this scenario, the position of the piezoelectric layer was considered near the clamp since $d_p = 0$ for all cases. That is why the vector of design variables was stipulated as $\boldsymbol{x}_d = \{l_v, R_c, h_p, l_p/l_c\}$. For the uncertain parameters, only those with more influence on the response were used in the uncertain vector, according to the previous section, i.e., $\boldsymbol{x} = \{k_w, k_\theta, \zeta, h_c\}$. The boundary conditions for the design variables remain the same as the previous ones, as well as the mean values and dispersions for the uncertain parameters. The optimization procedure was similar to that of the previous sections, choosing the PCE-3 with NSGA-II, using 50 individuals and 300 generations. The number of samples to determine the coefficients in PCE-3 was similar to the second scenario.

# 6 Comparison between the different designed devices

Succinctly, the three scenarios presented in before sections are analyzed in this results section, aiming to choose different energy harvesting devices. Scenario 1 focus on design variables, scenario 2 focus on uncertain parameters and scenario 3 focus on the most influential variables and parameters. It is intended to present the devices of scenarios 1, 2 and 3 in a unique Pareto front and another of error bars, evaluating performance issues, robustness and probability that one device will be better than another.

Particularly, for scenario 3, in which the most influential variables and parameters are considered, a more detailed analysis is presented in Tab. 2. These results are from a few devices only, after the convergence of the solutions in blue to the Pareto front shown in Fig. 3. It is possible to notice from the table that better mean performances were achieved with devices with shorter beams lengths, larger tip masses and thicker piezoelectric layers. On the contrary, longer beams, smaller tip masses and thinner piezoelectric layers lead to nominally worse but more robust performances. Also, reducing the effective resistance may increase robustness without much loss in mean performance. For example, there was an approximate reduction of 5.7% in the mean, while the dispersion was reduced by approximately 39%, evaluating the 2nd device in relation to the 1st device, decreasing mainly the electrical resistance .

Figure 3 shows the Pareto fronts for scenario 1, scenario 2 and scenario 3. An interesting analysis on these fronts concerns the dominance criterion in the case of better performance (higher mean) and lower relative dispersion. Although the points in Fig. 3 refer to different problems, a device-by-device dominance analysis between the other fronts can help in deducing some conclusions. On Pareto fronts, devices 1 to 11 are arranged in descending order of power; device 1 has the highest mean power and device 11 the lowest. For scenario 3, the green marks are presented to show the smoothness of the front between devices 1 and 2.

Table 2. Devices optimized for design variables $l_v$, $R_c$, $h_p$ and $l_p/l_c$ and uncertain $k_w$, $k_\theta$, $\zeta$, $h_c$.

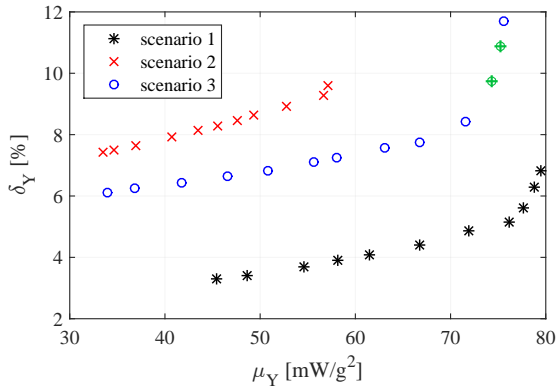| Device | $l_v$ (mm) | $h_b$ (mm) | $R_c$ (kΩ) | $h_p$ (mm) | $\frac{l_p}{l_v}$ | $\mu_Y$ mW/g$^2$ | $\delta_Y$ (%) |
|--------|------|------|------|------|------|------|------|
| #1 | 65.0 | 27.2 | 210.4 | 0.25 | 1.00 | 75.6 | 11.7 |
| #2 | 65.0 | 26.5 | 120.0 | 0.25 | 0.90 | 71.5 | 8.4 |
| #3 | 65.0 | 24.2 | 96.2 | 0.22 | 0.80 | 66.7 | 7.7 |
| #4 | 66.1 | 22.1 | 93.2 | 0.19 | 0.81 | 63.1 | 7.6 |
| #5 | 66.0 | 19.4 | 69.1 | 0.15 | 0.80 | 58.1 | 7.2 |
| #6 | 68.1 | 18.3 | 66.8 | 0.15 | 0.80 | 55.7 | 7.1 |
| #7 | 69.8 | 16.0 | 53.4 | 0.13 | 0.80 | 50.8 | 6.8 |
| #8 | 73.8 | 14.2 | 53.7 | 0.14 | 0.80 | 46.6 | 6.6 |
| #9 | 77.0 | 12.2 | 52.0 | 0.13 | 0.80 | 41.8 | 6.4 |
| #10 | 82.3 | 10.1 | 48.7 | 0.14 | 0.80 | 36.9 | 6.2 |
| #11 | 85.0 | 8.9 | 47.7 | 0.13 | 0.80 | 33.9 | 6.1 |



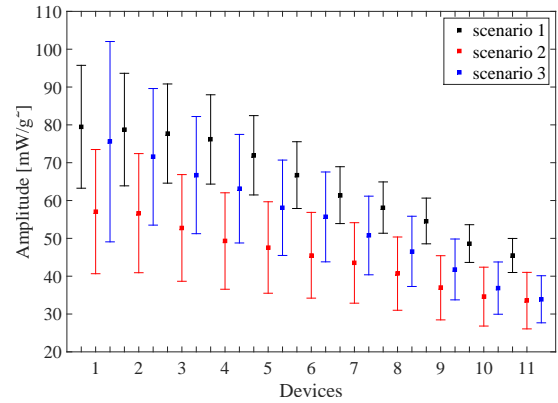Figure 3. Comparison of different devices designed using Pareto front



Figure 4. Comparison of different devices designed using error bars

Figure 4 represents the error bars of devices, with a tolerance of $3\sigma$. The nominally best device is not the best choice based on a worst-case scenario due to its worse robustness. For example, the best choice considering a worst-case would be device 2 in scenario 3, since its lower bound for the power output is the highest. But, notice that devices 3 and 4 may also be more interesting than device 1. From figures 3 and 4 is possible to observe that the devices of scenario 1, without uncertainty in the adhesive layer, are more likely to be better than the others. Therefore, the devices in scenario 2, without adding other design variables, tend to be worse or probabilistically have a lower power generated than the other cases. The devices of scenario 3 behave in an intermediate manner to the previous scenarios. From this, it is clear the importance of considering a reasonable amount of design variables in the optimization, and the effect of uncertainty in the clamp and the adhesive layer, given that disregarding uncertainties can lead to overestimated results. Regarding choosing one device or another, a subjective criteria will base the decision-making, depending on the conditions and feasibility that the analyst will have to assemble the prototype. Based on the analysis, a better strategy can be taken, from the choice of beam length, chosen seismic mass, placement of the piezoelectric insert, care with its adhesive layer and fixing of the device in the clamp.

## 7 Conclusions

This work presented the design of robust energy harvesting devices using multiobjective optimization via NSGA-II with polynomial chaos expansion to estimate statistical moments. Different scenarios were presented to

show how design variables and uncertain parameters affect the response of designed devices. With the increase of uncertainties in the parameters, it is important to consider a reasonable amount of design variables, so that the final devices have better performance and robustness. Furthermore, devices with shorter beam lengths and higher seismic mass showed better mean performance, while those with larger beams and smaller seismic mass were more robust. Finally, electrical resistances with values lower than the optimum lead to more robust devices, although the mean power may decrease slightly.

**Authorship statement.** The authors hereby confirm that they are the sole liable persons responsible for the authorship of this work, and that all material that has been herein included as part of the present paper is either the property (and authorship) of the authors, or has the permission of the owners to be included here.

# References

[1] N. E. Dutoit, B. L. Wardle, and S.-G. Kim. Design considerations for mems-scale piezoelectric mechanical vibration energy harvesters. *Integrated ferroelectrics*, vol. 71, n. 1, pp. 121–160, 2005.

[2] T. C. Godoy and M. A. Trindade. Effect of parametric uncertainties on the performance of a piezoelectric energy harvesting device. *Journal of the Brazilian Society of Mechanical Sciences and Engineering*, vol. 34, pp. 552–560, 2012.

[3] V. R. Franco and P. S. Varoto. Parameter uncertainties in the design and optimization of cantilever piezoelectric energy harvesters. *Mechanical Systems and Signal Processing*, vol. 93, pp. 593–609, 2017.

[4] G. I. Schuëller and H. A. Jensen. Computational methods in optimization considering uncertainties–an overview. *Computer Methods in Applied Mechanics and Engineering*, vol. 198, pp. 2–13, 2008.

[5] H.-S. Beyer and B. Sendhoff. Robust optimization–a comprehensive survey. *Computer methods in applied mechanics and engineering*, vol. 196, n. 33-34, pp. 3190–3218, 2007.

[6] K. Deb, A. Pratap, S. Agarwal, and T. Meyarivan. A fast and elitist multiobjective genetic algorithm: Nsga-ii. *IEEE Transactions on evolutionary computation*, vol. 6, n. 2, pp. 182–197, 2002.

[7] R. T. Marler and J. S. Arora. Survey of multi-objective optimization methods for engineering. *Structural and multidisciplinary optimization*, vol. 26, n. 6, pp. 369–395, 2004.

[8] H. F. L. Santos. Structural vibration control using piezoceramics in extension and shear connected to hybrid active-passive circuits (in portuguese). Master's thesis, University of São Paulo, 2008.

[9] B. B. Sudret. Polynomial chaos expansions and stochastic finite element methods. *Risk and reliability in geotechnical engineering*, pp. 265–300, 2014.

[10] S. S. Rao. *Engineering optimization: theory and practice*. John Wiley & Sons, 2009.

[11] P. H. Martins, M. A. Trindade, and P. S. Varoto. Simplified robust and multiobjective optimization of piezoelectric energy harvesters with uncertain parameters. *International Journal of Mechanics and Materials in Design*, vol. 18, n. 1, pp. 63–85, 2022.